Proceedings of the International Conference on Mining, Material and Metallurgical Engineering
Prague, Czech Republic, August 11-12, 2014
Keynote Lecture II

Manganese Diffusion in Third Generation Advanced High Strength Steels

Emmanuel De Moor*, Singon Kang, John G. Speer and David K. Matlock
Advanced Steel Processing and Products Research Center
Colorado School of Mines
1500 Illinois Street, Golden, CO-80401, USA
edemoor@mines.edu; sikang@mines.edu; jspeer@mines.edu; dmatlock@mines.edu

Abstract -Third generation advanced high strength steels (AHSS) are of importance to the automotive industry since their successful development may lead to further vehicle weight reduction, reduced fuel consumption and enhanced occupant protection. Promising properties have been generated through intercritical annealing of low-carbon manganese transformation induced plasticity steels. Austenite stabilization results from carbon and manganese enrichment and ultra-fine duplex ferrite/austenite microstructures are obtained. The present contribution uses DICTRA modeling to predict austenite retention from manganese and carbon diffusion. Significantly lower austenite fractions than experimentally observed are predicted, suggesting the importance of expanding diffusion models to incorporate diffusion contributions of high crystal imperfection densities including dislocations and grain boundaries which may significantly impact diffusional processes.

***Keywords*:** Third generation AHSS, Austenite, Medium manganese low-carbon TRIP steels.

1. Introduction

Significant research and industrial implementation efforts are underway to develop products with improved tensile property ranges identified as “Third Generation AHSS”. Increased consumer expectations and regulatory pressure (United States Environmental Protection Agency, 2012) are driving these materials needs and one original equipment manufacturer (OEM) has identified target ultimate tensile strength/total elongation combinations of 1000 MPa/30 pct and 1500 MPa/20 pct enabling potential body in white weight savings of 20 pct. A US Department of Energy integrated computational materials engineering (ICME) program has put forward even more aggressive target properties of 1200 MPa/30 pct and 1500 MPa/25 pct (Hector et al., 2013).

A review of recent research on AHSS steel developments (e.g. De Moor et al., 2010) indicates that a number of approaches show great potential to achieve third generation AHSS tensile properties including austempered bainitic alloys, quenching and partitioning (Q&P) and intercritical annealing of low-carbon manganese transformation induced plasticity (TRIP) steels (Grange et al., 1977; Merwin, 2008; and Miller, 1972). The generated microstructures in these approaches contain significant fractions of austenite believed to be crucial to obtain tensile ductility levels of interest (Matlock et al., 2006 and 2009). Austenite retention is obtained by solute enrichment during processing, thereby lowering the martensite start temperature (M_s) of the enriched austenite. Thermodynamic considerations have led to effective concepts in predicting carbon stabilized austenite levels including the T_o concept for austempering (Bhadeshia, 2011) and constrained carbon equilibrium (CCE) for Q&P (Speer et al., 2004).

Low-carbon manganese TRIP steels are gaining renewed attention as a potential third generation AHSS concept (Merwin, 2008; Jun et al., 2011; and Yulong et al., 2013). Early compositions encompass 0.1 wt pct carbon and 4 to 7 wt pct manganese and heat treating involves intercritical annealing to enrich austenite with manganese. A straightforward model to predict austenite stabilization through manganese enrichment during intercritical annealing assuming orthoequilibrium is reviewed in the present contribution in addition to diffusional considerations.

2. Austenite Stabilization through Manganese Enrichment

Intercritical annealing of medium manganese steels has shown effective in stabilizing substantial amounts of austenite (Grange et al., 1977; Merwin, 2008; Jun et al., 2011 and Gibbs et al., 2011) and generating attractive properties. Most experimental studies however reveal a significant sensitivity to annealing temperatures and times. In particular the tensile properties are very dependent on annealing temperature fluctuations and very narrow processing window tolerances would currently be crucial for industrial implementation. This may limit product implementation and it is hence crucial to better understand this annealing response sensitivity.

An initial effort to predict austenite retention as a function of annealing temperature has been conducted using a straightforward model (De Moor et al., 2011). Austenite fractions stable at room temperature following intercritical annealing are predicted by assuming equilibrium partitioning of manganese and carbon in ferrite and austenite. The methodology used involves prediction of the ferrite/austenite fractions using Thermo-Calc^{TM} along with their respective equilibrium manganese and carbon contents in the intercritical region. The M_s temperature of the enriched austenite is then calculated according to

M_s = 539-423C-30.4Mn-7.5Si+30Al (Mahieu et al., 2002) (1)

and prediction of the amount of fresh martensite formed upon cooling below the M_s temperature to room temperature can be calculated based on the Koistinen Marburger (KM) equation:

$$f_M = 1 - e^{-k(M_s - T)} \qquad (2)$$

with k a constant, with a typical value of 0.011. Subtraction of the predicted “fresh” martensite formed during the final quench to room temperature from the austenite fraction predicted to be present at the annealing temperature hence yields the final retained austenite fraction present at room temperature stabilized by carbon and manganese enrichment.

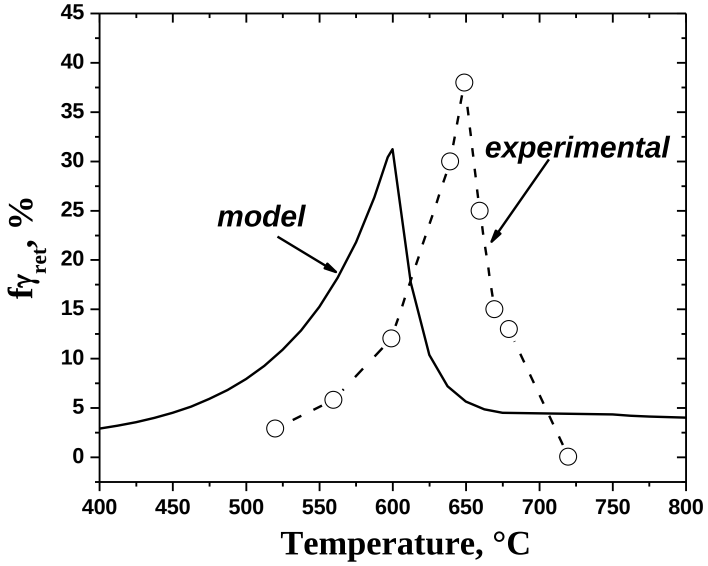

Fig. 1. Retained austenite fractions predicted in a 0.1C-6Mn composition assuming equilibrium Mn partitioning between ferrite and austenite and experimental data obtained after isothermal intercritical annealing for one hour reported by Miller, 1972.

Fig. 1 shows the results of predicted austenite fractions for a 0.1C-6Mn composition using the model and also plots experimental data obtained by Miller (1972) using one hour isothermal holds. When comparing the modeled and experimental values, it is apparent that a similar trend as a function of annealing temperature is obtained, albeit that the peak experimental fractions are greater than predicted and that the predicted peak temperature is lower.

2. Diffusional Considerations

The initial modeling approach assumes equilibrium fractions and, in order to incorporate diffusion kinetics, DICTRA^{TM} simulations were employed to calculate manganese diffusion fronts in ferrite and austenite. A one-dimensional approach was taken by defining adjacent bcc and fcc cells and dimensional assumptions are schematically shown in Fig. 2. Fig. 2a shows half widths of ferrite and austenite proportional in size to the volume fraction of each phase predicted to be present at the intercritical annealing temperature by Thermo-Calc calculations. The total of both half widths was chosen constant and equal to experimental average grain sizes obtained following intercritical annealing, which are reported to be strongly dependent on annealing temperature (Miller, 1972 and Lee et al., 2010). Current literature data does not distinguish between ferrite and austenite grain size. The bcc/fcc interface was assumed immobile and carbon and manganese solute was allowed to diffuse.

DICTRA calculations were performed for temperatures of 600, 650 and 700 °C and times of 1, 5, 30, 60, 120, 180, 300, 900, 1800 and 3600 s. The grain sizes derived from literature data (Miller, 1972 and Lee et al., 2010) phase volume fractions from Thermo-Calc calculations, and corresponding cell sizes used as input parameters are given in Fig. 2b. The resulting manganese profiles obtained from 650 °C simulations are given in Fig. 3 and suggest that manganese diffusion was insufficient to stabilize the austenite. The increased manganese levels in the austenite are predicted to be confined to a very narrow band in the austenite cell due to the much lower diffusivity in austenite.

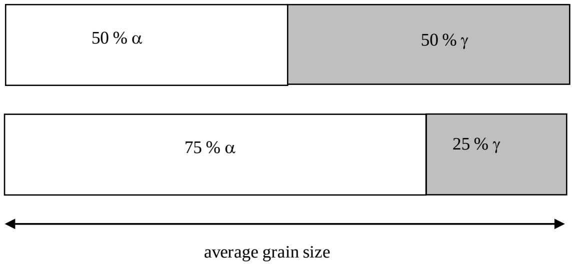

a)

T, °C	grain size, μm	f_γ, vol%	cell size α, μm	cell size γ, μm
600	0.39	31	0.2691	0.1209
650	0.47	49	0.2397	0.2303
700	0.54	83	0.0918	0.4482

b)

Fig. 2. Schematic illustration of microstructural input parameters for DICTRA modeling. The half width of ferrite and austenite are shown and are proportional to their relative volume fractions. The total length of the two cells is chosen equal to experimental average grain sizes shown in b) along with phase volume fractions from Thermo-Calc calculations, and corresponding cell sizes used as input parameters.

In order to predict the volume fraction of austenite stable at room temperature based on the manganese profiles shown in Fig. 3b, a methodology proposed by Clarke et al. (2009) to predict retained austenite stabilized by solute carbon enrichment was employed. In this approach it is assumed that martensite can nucleate on a solute diffusion front if the local M_s temperature is above room temperature and the Koistinen-Marburger equation may be applied locally to the solute diffusion front. The M_s temperature was calculated and the KM equation applied for each point of the profile shown in Fig. 3b and the resulting “local” stable austenite fraction is determined as shown in Fig. 4a. Integration of the area under this curve yields the predicted stable austenite fraction of the austenite present at the annealing temperature and the total volume percent stable austenite fraction can be calculated. Since the diffusion of interstitial carbon is much faster than manganese, equilibrium carbon contents were assumed for calculations. The resulting austenite volume fractions stabilized by manganese enrichment and assuming equilibrium carbon contents are shown in Fig. 4b as a function of annealing time. It is clear from Fig. 4b that the austenite fractions predicted for equilibrium manganese partitioning are not stabilized for annealing times up to one hour. The experimental fractions reported in Fig. 1 are also significantly greater.

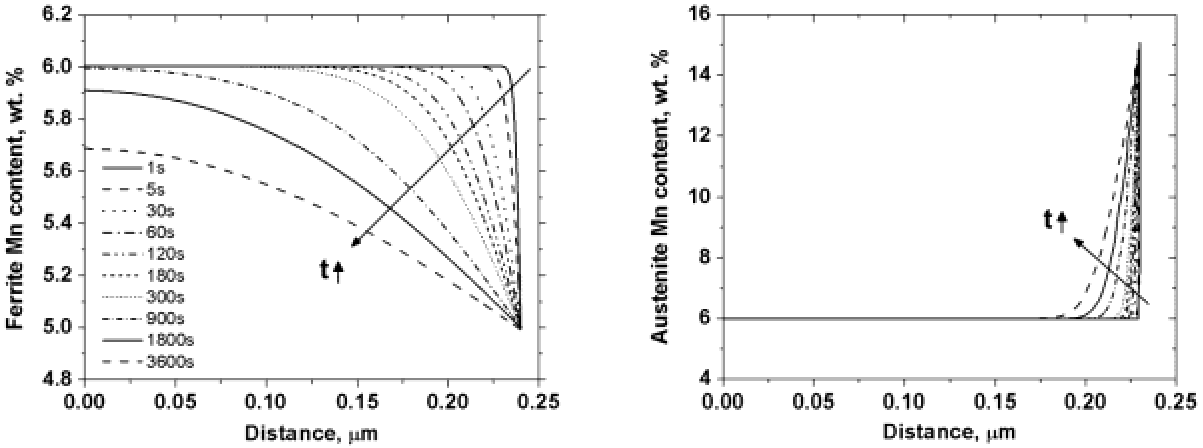

a) b)

Fig. 3. Manganese profiles in a) ferrite and b) austenite calculated for 650 °C in a 0.1C-6Mn composition for 1, 5, 30, 60, 120, 180, 300, 900, 1800 and 3600 s based on the input parameters shown in Fig. 3b. The interface is at the right hand side in both figures.

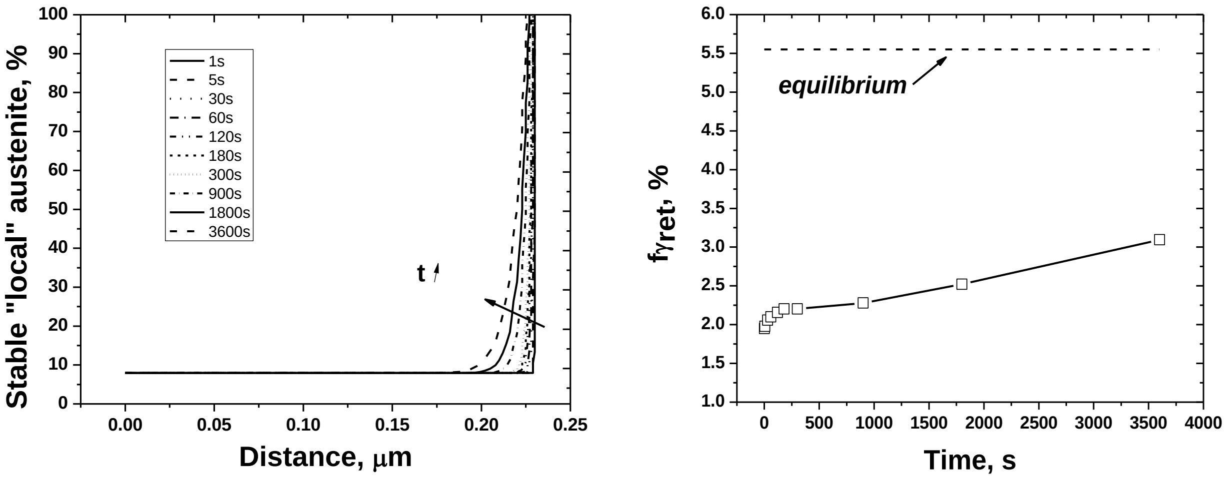

a) b)

Fig. 4. a) Stable “local” austenite predicted by applying the KM equation to the local manganese profile b) Calculated austenite fractions as a function of time for the 0.1C-6Mn steel and an annealing temperature of 650 °C. The austenite level predicted assuming equilibrium manganese levels is also given.

Further calculations were conducted for annealing temperatures of 600 and 700 °C using the input parameters shown in Fig. 3b and the results are plotted in Fig. 5. It is clear from Fig. 5 that the calculated values are lower than the values obtained when equilibrium is assumed for all temperatures. Experimental values reported by Miller (1972) for one hour isothermal annealing are also shown as well as experimental values obtained by Lee et al. (2011) for a 0.05C-6.15Mn-1.50Si steel. Three minute intercritical anneals were used in this study and significant fractions up to 30 vol pct were measured by X-ray diffraction. It is hence clear that significant fractions are experimentally obtained even for short annealing times at levels far greater than calculated using the approach outlined above.

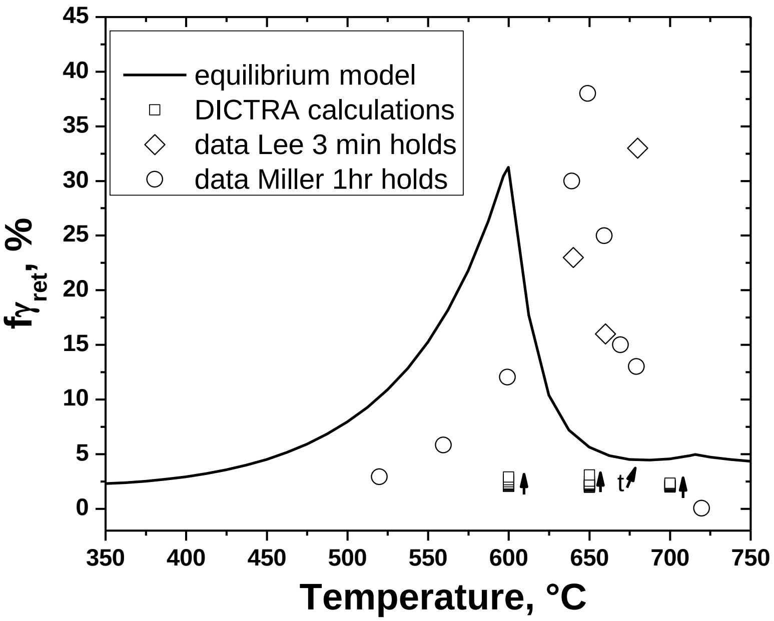

Fig. 5. Calculated stable austenite fractions for times ranging from 1 to 3600 s based on manganese profiles obtained from DICTRA calculations and assuming equilibrium carbon content plotted as a function of annealing temperature. Predicted austenite fractions assuming equilibrium solute contents (De Moor et al., 2011) and experimental data reported by Lee et al. (2011) and Miller (1972) are also shown.

Diffusion data in the DICTRA databases are based on diffusion in ferrite. It should however be noted that the hot rolled microstructure of medium Mn steels is reported to be martensitic (Merwin, 2008) and the high dislocation density of the martensite may significantly impact diffusivity (Hart, 1957) since a more “open” structure may perhaps provide faster diffusion paths for substitutional diffusion somewhat similar to pipe diffusion i.e. diffusion along grain boundaries. In addition, the high density of lath boundaries in the martensitic packets of the starting microstructure may further accelerate manganese diffusion. It is of interest to note that recent atom probe work performed on a 0.05C 12Mn-2Ni-0.6Mo-1.2Ti at pct maraging steel suggests a much greater diffusion of manganese in martensite (Dmitrieva et al., 2011) and diffusion constants up to 45 times greater than the diffusion of manganese in bcc iron are suggested to better correspond to experimental manganese diffusion profiles obtained at a martensite/austenite interface for an annealing at 450 °C. The suggested increased diffusivity might help explain the increased retained austenite fractions observed after a few minutes of annealing observed by Huang et al. (1994) and Lee et al. (2011).

3. Conclusions

Since low-carbon manganese TRIP steels are under increased attention to reach third generation AHSS property targets, an improved understanding of manganese diffusion mechanisms during intercritical annealing is needed. The present contribution used DICTRA modeling assuming a stationary interface with dimensional assumptions based on predicted phase fractions and application of the Koistinen-Marburger equation on a diffusing solute front to predict austenite retention. Predicted values are significantly lower than experimentally observed fractions indicating a need to incorporate diffusion contributions from grain boundaries and dislocations. Improved predictive capabilities will accelerate the development and potential industrial implementation of these steels.

Acknowledgements

The authors gratefully acknowledge the support of the sponsors of the Advanced Steel Processing and Products Research Center, an industry/university cooperative research center at the Colorado School of Mines.

References

Bhadeshia H.K.D.H. (2001). “Bainite in Steels” Institute of Materials.

Clarke A.J., Speer J.G., Matlock D.K., Rizzo F.C., Edmonds D.V., Santofimia M.J. (2009). Influence of Carbon Partitioning Kinetics on Final Austenite Fraction during Quenching and Partitioning. Scripta Mat., 61, 149-152.

De Moor E., Matlock D.K., Speer J.G., Merwin M.J. (2011). Austenite Stabilization through Manganese Enrichment, Scripta Mater., 64, 185-188.

De Moor E., Speer J.G., Matlock D.K. (2010). Strategies for Third-Generation Advanced High-Strength Steel Development. AIST Transactions, 7, 133-144.

Dmitrieva O., Ponge D., Inden G., Millán J., Choi P., Sietsma J., Raabe D. (2011). Chemical Gradients Across Phase Boundaries between Martensite and Austenite in Steel Studied by Atom Probe Tomography and Simulation. Acta Mater., 59, 364-374.

Gibbs P.J., De Moor E., Merwin M.J., Clausen B., Speer J.G., Matlock D.K. (2011). Austenite Stability Effects on Tensile Behavior of Manganese-Enriched- Austenite Transformation-Induced Plasticity Steel. Metall. Trans. A, 42, 3691-3702.

Grange R.A., Miller R.L. (1977). Heat Treatment for Improving the Toughness of High-Manganese Steels. U.S. Patent 4047979 A.

Hart E.W. (1957). On the Role of Dislocations in Bulk Diffusion. Acta Metall., 5, 597.

Hector L.G. Jr., Krupitzer R., Sachdev A.K. (2013). Integrated Computational Materials Engineering (ICME) for Third Generation Advanced High-Strength Steels: A New Four-Year Project. “Proc. Intl. Symp. on New Develop. inAdvanced High-Strength Sheet Steels,” Vail, CO, Jun. 23–27, pp. 341-349.

Huang H., Matsumura O., Furukawa T. (1994). Retained Austenite in Low Carbon, Manganese Steel after Intercritical Heat Treatment. Mater. Sci. and Tech., 10, 621-626.

Jun H.J., Yakubovsky O., Fonstein N. (2011). On Stability of Retained Austenite in Medium Mn TRIP Steels. “Proc. of the 1st Intl. Conf. on High Manganese Steels,” Seoul, Korea, May 15-18, pp.A-5-1–A-5-13.

Lee S., Lee K., De Cooman B.C. (2010). Ultra-fine Grained 6wt% Manganese TRIP Steel. Materials Sci. For., 654-656, 286-289.

Lee S., Lee S.-J., Kumar S.S., Lee K., De Cooman B.C. (2011). Localized Deformation in Multiphase, Ultra-Fine-Grained 6 Pct Mn Transformation Induced Plasticity Steel. Metall. and Mater. Trans. A, 42, 3638-3651.

Mahieu J., Maki J., De Cooman B.C., Claessens S. (2002). Phase Transformation and Mechanical Properties of Si-Free CMnAl Transformation-Induced Plasticity-Aided Steel. Metall. Trans. A, 33, 2573-2580.

Matlock D.K., Speer J.G. (2006). Design Considerations for the Next Generation of Advanced High-Strength Sheet Steels. “Proc. of the 3rd Inter. Conf. on Structural Steels,” Gyeongju, Korea, August 22-24, pp. 774–781.

Matlock D.K., Speer J.G. (2009). Third Generation of AHSS: Microstructure Design Concepts. “Proc. of the Inter. Conf. on Microstructure and Texture in Steels and Other Materials,” London, England, Feb. 5-7, pp. 185-205.

Merwin M.J. (2008). Microstructure and Properties of Cold Rolled and Annealed Low-Carbon Manganese TRIP Steels. Iron & Steel Technology, 5, 66-84.

Miller R.L. (1972). Ultrafine-Grained Microstructures and Mechanical Properties of Alloy Steels. Metall. Trans. A, 3, 905-912.

Speer J.G., Matlock D.K., De Cooman B.C., Schroth J.G. (2004). Comments on “On the Definitions of Paraequilibrium and Orthoequilibrium” by M. Hillert and J. Ågren, Scripta Materialia, 50, 697-9 (2004), Scripta Mater., 52, 83-85.

United States Environmental Protection Agency, Department of Transportation (2012). 2017 and Later Model Year Light-Duty Vehicle Greenhouse Gas Emissions and Corporate Average Fuel Economy Standards. Federal Register, 77, pp. 62623-63200.

Yulong Z., Hua W., Jiyao H., Li W. (2013). “Dependence of Mechanical Properties on Annealing Parameters in Medium-Mn TRIP Steels. “Proc. Intl. Symp. on New Developments in Advanced High-Strength Sheet Steels,” Vail, CO, Jun. 23–27, pp. 351-360.